

HeTDSE: GPU based program to solve full-dimensional-time-dependent Schrödinger equation for two-electron Helium subjected to strong laser fields

Changli Wei¹ and Xi Zhao^{2*}

¹ *School of physics and electronics,*

Qiannan Normal College For Nationalities, Duyun City,

Guizhou Province 558000, People's Republic of China and

² *Department of Physics, Kansas State University, Manhattan, KS 66506, USA*

(Dated: November 20, 2019)

Abstract

We present a GPU based openACC fortran program named HeTDSE, which provides an efficient way to investigate the non-perturbative electronic dynamics of helium subjected to a strong laser pulse by solving full-dimensional two-electron time dependent Schrödinger equation (TDSE). OpenACC is a directive-based programming model for accelerators without modifying the underlying CPU code itself. HeTDSE uses B-Spline basis sets expansion method to construct the radial part of the wavefunction, and the spherical harmonic functions is used to express for the angular part. Adams algorithm is employed for the time propagation. Our example shows HeTDSE running on an NVIDIA Kepler K20 GPU can outperform the one on an Intel E5-2640 single CPU core by a factor of 147.

PACS numbers: 32.80.Rm, 42.50.Hz, 42.65.Ky

* zhaoxi719@ksu.edu

Program summary

Program Title: HeTDSE

Programming language: Fortran, openACC.

Licensing provisions: GNU General Public License 3 (GPLv3).

Computer: All computers with a Fortran compiler with an openACC-enable accelerator. Even a desktop computer with an openACC-enable accelerator can run HeTDSE.

Operating system: No limits.

Has the code been parallelized?: This program is able to run both in sequential and parallel mode. For parallel running, the code is parallelized by openACC (GPU based parallel implementation) and openMP (CPU based parallel implementation).

Nature of problem: Electron-electron correlation plays an important role in the underlying dynamics in physics and chemistry. Helium is the simplest and most fundamental two-electron system. The dynamic process of helium in a strong laser field is still a challenging issue because of the large calculation cost. In this study, a GPU openACC based *ab initio* numerical simulations code is developed to solve the full dimensional time-dependent Schrödinger equation of helium subjected to a strong laser pulse.

Solution method: HeTDSE codes uses B-Spline basis sets to construct the radial part of the wavefunction, and the spherical harmonic functions is used to express for the angular part. We convert the TDSE into coupled partial differential equations. Adams algorithm is employed for the time propagation. The simulations are performed using parallel GPU implementations.

Running time: The running time depends on the number of B-Spline basis functions, the duration of the laser pulses, and the number of GPUs/CPUs. Depending on these factors, it can vary between minutes and weeks.

Restrictions: The present program is restricted to linearly polarized light. Besides, the number of basis sets is limited depending on the memory of the accelerator.

I. INTRODUCTION

The rapid development of the free-electron-laser-pulse technology [1, 2] and the application of high order harmonic generation (HHG) [3, 4] opens a way to investigate the ionization processes of atoms and molecules by high frequency laser pulse. Recently, the dynamics of

helium in a strong laser field has attracted a lot of attention [5–12, 14–19]. In recent years, conventional CPU parallel computing technique makes it possible to numerically solve the TDSE of helium subjected to a laser pulse. Peng *et al.* investigated the electron correlation effects in two-photon-double-ionization (TPDI) of helium by finite-element-discrete-variable-representation (FEDVR) method [20]; Parker *et al.* used the finite-difference method to calculate the above threshold ionization (ATI) process [21]; Piraux *et al.* investigated the electron correlation effect by using the Gauss-Sturman function [10]. However, for the calculation cost is large in these studies, the simulations are particularly numerically expensive (about 200 to 1000 CPU cores are used [20, 21]). It is very likely a numerical virtual experiment on the servers [21]. More efficient calculation method and low-cost compute device are the two keys to further promoting the numerical simulations in strong laser field investigations. To achieve these aims, high performance computing technique has been widely applied in numerically studies, such as graphic processing unit(GPU) [23].

GPU contains hundreds of computing cores and is originally designed for the highly parallel process of graphic rendering [22, 23]. In recent twenty years, GPU has evolved into a very powerful and low-cost compute device in science and engineering [24]. Comparing with CPU, the performance of GPU implementations increases by tens of times [23–29]. Especially, the Compute Unified Device Architecture (CUDA) is one of the most widely used programming model for accelerators [23]. However, the programming for accelerators such as CUDA is difficult to master and usually combines the programming code to an accelerators of a particular hardware parameter. This leads to the highly hardware-specific dependence, and those dependencies will cause a lack of the expansibility of the code[24]. To overcome these difficulties, OpenACC is proposed as a standard programming model for accelerators [30]. OpenACC is a set of directive-based extensions to C, C++ and Fortran that allow programmers to annotate regions of code and data for offloading from a CPU host to an attached Accelerator, without requiring modification to the underlying CPU code itself. A typical fortran openACC program is shown in Fig 1:

Programmers simply insert OpenACC directives "acc parallel loop" before specific code sections with the do loop, to engage the GPU. This approach enables the compiler to target and optimize parallelism [30].

Besides the computing cost, how to get the continue states is another challenge in investigations of matter-laser interaction [31]. As shown in [32], B-spline basis sets, which were

widely used in computational atomic and molecular physics [32–35], has great advantages of describing the continue states: the density of discretized continuum states can be adjusted with a total degree of freedom simply by modifying the box size [32]. For this reason, we introduce the B-Spline basis sets to construct the radial part of the wavefunction in this work. We expand the time dependent Helium wavefunction as a set of B-Spline functions, then we convert the TDSE into coupled partial differential equations. The expansion coefficients at each time step can be got. In principle, if we have the expansion coefficients, all the physical process can be retrieved.

The paper is organized as follows: In section 2, we present the theoretical background on which the codes is built. In Section 3 we exhibit an overview of the package structure, the input and output files. In Section 4 we show several test applications of HeTDSE. The parallel efficiency is given in Section 5. We present our conclusions in Section 6.

II. MATHEMATICAL SETUP AND ALGORITHM

We solve the Helium TDSE within dipole approximation and length gauge. Atomic units are used throughout, unless otherwise stated. The full-dimension-TDSE of helium is

$$i\frac{\partial}{\partial t}\Psi(\mathbf{r}_1, \mathbf{r}_2, t) = H(\mathbf{r}_1, \mathbf{r}_2, t)\Psi(\mathbf{r}_1, \mathbf{r}_2, t), \quad (1)$$

where the total Hamiltonian of atom-laser system is

$$H(\mathbf{r}_1, \mathbf{r}_2, t) = -\frac{\nabla_1^2}{2} - \frac{\nabla_2^2}{2} - \frac{2}{\mathbf{r}_1} - \frac{2}{\mathbf{r}_2} + \frac{1}{|\mathbf{r}_1 - \mathbf{r}_2|} + H_I(t), \quad (2)$$

where $-\nabla_i^2/2 - 2/r_i$ with $i = 1, 2$ denotes the kinetic energy and potential energy of electron i , and $\frac{1}{|\mathbf{r}_1 - \mathbf{r}_2|}$ is the electron-electron correlation term. The interaction Hamiltonian of the helium and laser pulse is

$$H_I(t) = (\mathbf{r}_1 + \mathbf{r}_2) \cdot \mathbf{e}(\mathbf{t}) = -(\mathbf{r}_1 + \mathbf{r}_2) \cdot \partial \mathbf{A}(\mathbf{t}) \partial t, \quad (3)$$

where the vector potential of the laser pulse is

$$\mathbf{A}(\mathbf{t}) = \hat{\varepsilon} A_0 \exp(-\alpha^2 t^2) \sin(\omega t + \phi) / \omega, \quad (4)$$

where $\hat{\varepsilon}$ is the laser polarization direction, ω and ϕ are the frequency and the carrier envelope phase, respectively. $\alpha = \frac{\sqrt{2 \ln(2)}}{\tau}$, with τ being the Full-Width-Half-Maximum

(FWHM). The wavefunction of helium can be written as

$$\Psi(\mathbf{r}_1, \mathbf{r}_2, t) = \sum_n a_n(t) e^{-iE_n t} \varphi_n(\mathbf{r}_1, \mathbf{r}_2), \quad (5)$$

where the time-independent Helium wavefunction is

$$\begin{aligned} \varphi_n(\mathbf{r}_1, \mathbf{r}_2) = & \sum_{i=1}^N c_i [B_{n_1}(r_1) B_{n_2}(r_2) Y_{l_1 l_2}^{LM}(\hat{r}_1, \hat{r}_2) \\ & + (-1)^{l_1+l_2+L} B_{n_1}(r_2) B_{n_2}(r_1) Y_{l_1 l_2}^{LM}(\hat{r}_2, \hat{r}_1)] \end{aligned}, \quad (6)$$

where $B_{n,k}(r)$ is a B-Spline of order k (in our calculation $k = 7$, so we don't write out k in B-Spline functions), which can be defined as

$$\begin{aligned} B_{j,1}(r) &= \begin{cases} 1 & t_j \leq r \leq t_{j+1}, \\ 0 & \text{otherwise} \end{cases} \\ B_{j,k}(r) &= \frac{r-t_j}{t_{j+k-1}-t_j} B_{j,k-1} + \frac{t_{j+k}-r}{t_{j+k}-t_{j+1}} B_{j+1,k-1}, \end{aligned} \quad (7)$$

where $\{t_j\}$ denotes the spline knot sequence. N is the number of the basis sets, and each i corresponds to a set of $\{n_1, l_1, n_2, l_2\}$.

$$\begin{aligned} Y_{l_1 l_2}^{LM} &= \sum_{m_1 m_2} (-1)^{l_1-l_1+L} \sqrt{2L+1} \begin{pmatrix} l_1 & l_2 & L \\ m_1 & m_2 & -M \end{pmatrix} \\ &\times Y_{l_1 m_1}(\hat{r}_1) Y_{l_2 m_2}(\hat{r}_2), \end{aligned} \quad (8)$$

where $Y_{lm}(\hat{r})$ is usual spherical harmonic functions. L is the total orbital angular momentum and M is its z-component. We convert the TDSE into coupled partial differential equations:

$$i \frac{d}{dt} a_n(t) = \sum_m a_m(t) e^{-iE_{mn} t} H_{nm}^I(t), \quad (9)$$

where $E_{mn} = E_m - E_n$, $H_{nm}^I = \langle \varphi_m(\mathbf{r}_1, \mathbf{r}_2) | H^I(t) | \varphi_n(\mathbf{r}_1, \mathbf{r}_2) \rangle$ is the transition dipole, using $\cos \theta = \sqrt{\frac{4\pi}{3}} Y_{10}(\hat{r})$, we get

$$\begin{aligned} H_{nm}^I &= \sqrt{\frac{4\pi}{3}} E(t) \sum_{i,j} c_i c_j \langle \varphi_n | r_1 Y_{10}(\hat{r}_1) + r_2 Y_{10}(\hat{r}_2) | \varphi_m \rangle \\ &= \sqrt{\frac{4\pi}{3}} E(t) \sum_{i,j} c_i c_j (term1 + term2 + term3 + term4), \end{aligned} \quad (10)$$

where $termi = T_{i1} + T_{i2}$,

$$\begin{aligned}
T_{11} &= \langle \phi(n'_1, l'_1; n'_2, l'_2) | r_1 Y_{10}(\hat{r}_1) | \phi(n_1, l_1; n_2, l_2) \rangle \\
T_{12} &= \langle \phi(n'_1, l'_1; n'_2, l'_2) | r_2 Y_{10}(\hat{r}_1) | \phi(n_1, l_1; n_2, l_2) \rangle \\
T_{21} &= (-1)^S \langle \phi(n'_1, l'_1; n'_2, l'_2) | r_1 Y_{10}(\hat{r}_1) | \phi(n_2, l_2; n_1, l_1) \rangle \\
T_{22} &= (-1)^S \langle \phi(n'_1, l'_1; n'_2, l'_2) | r_2 Y_{10}(\hat{r}_2) | \phi(n_2, l_2; n_1, l_1) \rangle \\
T_{31} &= (-1)^{S'} \langle \phi(n'_2, l'_2; n'_1, l'_1) | r_1 Y_{10}(\hat{r}_1) | \phi(n_1, l_1; n_2, l_2) \rangle \\
T_{32} &= (-1)^{S'} \langle \phi(n'_2, l'_2; n'_1, l'_1) | r_2 Y_{10}(\hat{r}_2) | \phi(n_1, l_1; n_2, l_2) \rangle \\
T_{41} &= (-1)^{S+S'} \langle \phi(n'_2, l'_2; n'_1, l'_1) | r_1 Y_{10}(\hat{r}_1) | \phi(n_1, l_1; n_2, l_2) \rangle \\
T_{42} &= (-1)^{S+S'} \langle \phi(n'_2, l'_2; n'_1, l'_1) | r_2 Y_{10}(\hat{r}_2) | \phi(n_1, l_1; n_2, l_2) \rangle
\end{aligned} \tag{11}$$

In these equations, we can separate the radial part and the angular part,

$$T_{ij} = I_{ij} \times G_{ij}, i = 1, 2, j = 1, 2, \tag{12}$$

hence we can get the radial part easily by numerical integral,

$$I_{11} = \int dr_1^3 \int dr_2^3 B_{n'_1}(r_1) B_{n'_2}(r_2) r_1 B_{n_1}(r_1) B_{n_2}(r_2). \tag{13}$$

By using the quantum mechanics graph theory [36], the analysis expression of the angle part is

$$G_{11} = (-1)^{l_2+M'} \sqrt{\frac{(1, l_1, l'_1, L, L')}{4\pi}} \begin{pmatrix} 1 & l_1 & l'_1 \\ 0 & 0 & 0 \end{pmatrix} \begin{pmatrix} 1 & L' & L \\ 0 & 0 & 0 \end{pmatrix} \begin{Bmatrix} 1 & l_1 & l'_1 \\ l_2 & L' & L \end{Bmatrix}, \tag{14}$$

we use a convention $(a, b, c) = \sqrt{(2a+1)(2b+1)(2c+1)}$ in Eq. (14), other parts of Eq. (12) include

$$I_{12} = \int dr_1^3 \int dr_2^3 B_{n'_1}(r_1) B_{n'_2}(r_2) r_2 B_{n_1}(r_1) B_{n_2}(r_2), \tag{15}$$

$$G_{12} = (-1)^{l_1+M'} \sqrt{\frac{(1, l_2, l'_2, L, L')}{4\pi}} \times \begin{pmatrix} 1 & l_2 & l'_2 \\ 0 & 0 & 0 \end{pmatrix} \begin{pmatrix} 1 & L' & L \\ 0 & 0 & 0 \end{pmatrix} \begin{Bmatrix} 1 & l_2 & l'_2 \\ l_1 & L' & L \end{Bmatrix}, \tag{16}$$

$$I_{21} = \int dr_1^3 \int dr_2^3 B_{n'_1}(r_1) B_{n'_2}(r_2) r_1 B_{n_1}(r_2) B_{n_2}(r_1), \tag{17}$$

$$G_{21} = (-1)^{l_1+l_2+L+S} \times G_{11} (l_1 \leftrightarrow l_2), \tag{18}$$

$$I_{22} = \int dr_1^3 \int dr_2^3 B_{n'_1}(r_1) B_{n'_2}(r_2) r_2 B_{n_1}(r_2) B_{n_2}(r_1), \tag{19}$$

$$G_{22} = (-1)^{l_1+l_2+L+S} \times G_{12} (l_1 \leftrightarrow l_2), \tag{20}$$

$$I_{31} = \int dr_1^3 \int dr_2^3 B_{n'_1}(r_2) B_{n'_2}(r_1) r_1 B_{n_1}(r_1) B_{n_2}(r_2), \tag{21}$$

$$G_{31} = (-1)^{l'_1+l'_2+L'+S'} \times G_{11} \left(l'_1 \leftrightarrow l'_2 \right), \quad (22)$$

$$I_{32} = \int dr_1^3 \int dr_2^3 B_{n'_1}(r_2) B_{n'_2}(r_1) r_2 B_{n_1}(r_1) B_{n_2}(r_2), \quad (23)$$

$$G_{32} = (-1)^{l'_1+l'_2+L'+S'} \times G_{12} \left(l'_1 \leftrightarrow l'_2 \right), \quad (24)$$

$$I_{41} = \int dr_1^3 \int dr_2^3 B_{n'_1}(r_2) B_{n'_2}(r_1) r_1 B_{n_1}(r_2) B_{n_2}(r_1), \quad (25)$$

$$G_{41} = (-1)^{l'_1+l'_2+L'+S'+l_1+l_2+L+S} \times G_{11} \left(l'_1 \leftrightarrow l'_2, l_1 \leftrightarrow l_2 \right), \quad (26)$$

$$I_{42} = \int dr_1^3 \int dr_2^3 B_{n'_1}(r_2) B_{n'_2}(r_1) r_2 B_{n_1}(r_2) B_{n_2}(r_1), \quad (27)$$

$$G_{42} = (-1)^{l'_1+l'_2+L'+S'+l_1+l_2+L+S} \times G_{12} \left(l'_1 \leftrightarrow l'_2, l_1 \leftrightarrow l_2 \right), \quad (28)$$

where $f(a \leftrightarrow b)$ indicates that a and b exchange their positions in function f .

III. DESCRIPTION OF THE CODES

The HeTDSE is written in Fortran language. The codes give a convenient and efficient way to study the electronic dynamics of two-electron system Helium in a (strong) laser field. HeTDSE contains 9 fortran files and 4 input files. The fortran driver programs, functions, subroutines, input files and output files are introduced briefly in this section. The construction of HeTDSE can be found in Fig. 2, user should run these codes step by step: Firstly, user should run **eigen-equation.f** to get the initial wavefunction of helium; Then, using the output files of **eigen-equation.f**, user should run **dipole.f90** to get the transition dipoles; Next, using the output files of **dipole.f90**, user should run **matrix.f90** to generate the input files for **tdse.f90**; Finally, using the output files of **matrix.f90**, user should run **tdse.f90** to solve the Eq. (9) to get the time-dependent wavefunction of Helium.

A. *eigen-equation.f*

This program is used to get the expansion coefficient $\{c_i\}$ in Eq. (6) by solving the time independent two-electron full dimensional Schrödinger equation of Helium,

$$H(r_1, r_2) \Psi(r_1, r_2) = E \Psi(r_1, r_2), \quad (29)$$

where

$$H(r_1, r_2) = -\frac{\nabla_1^2}{2} - \frac{\nabla_2^2}{2} - \frac{2}{r_1} - \frac{2}{r_2} - \frac{1}{|r_1 - r_2|}. \quad (30)$$

The functions and subroutines in this program are:

PREQUAN: Get the index of the one electron functions $B_n(r) Y_{lm}$ from 1 to $n \times (l_{\max} + 1)$.

QUAN2012: Select the basis sets that satisfies physics considerations: the one electron angular momenta l_1, l_2 should satisfy $|l_1 - l_2| \leq L \leq |l_1 + l_2|$ and the wavefunction $\Psi(r_1, r_2) \neq 0$.

gauleg: Calculate the Gauss-Lagrange integration.

DBSP2: Calculate $\frac{\partial B_n^2(x)}{\partial x^2}$.

DBSP1: Calculate $\frac{\partial B_n(x)}{\partial x}$.

RKTSQ: Get the knot-point distribution. In our code, we set the distribution as the Linear-parabolic sequence.

$$\begin{aligned} r_0 &= \xi_{i_0} = \frac{r_{\max}(i_0-1) + r_{\min}(n-i_0)}{2n-i_0-1} \\ \alpha &= \frac{r_0 - r_{\min}}{(i_0-1)^2} \\ \beta &= \frac{r_{\max} - r_0}{n-i_0} \\ \xi_i &= \begin{cases} r_{\min} + \alpha(i-1)^2 & 1 \leq i < i_0 \\ r_0 + \beta(i-i_0) & i_0 < i \leq n \end{cases} \end{aligned} \quad (31)$$

Bspline2006: Calculate the B-Spline function $B_n(x)$.

SingleInteg2012: Calculate the integration $\int B_n(x) x B_m(x) dx$ and $\int B_n(x) B_m(x) dx$.

DmultiInteg2012: Calculate the electron-electron integration $\int B_n(r_i) \frac{1}{r_{ij}} B_m(r_j) dx$.

HAMILTON2012: Construct the Hamiltonian.

RSG: Diagonalize the matrix, get the energy level and wavefunctions.

Input file of eigen-equation.f:

eigen-equation.input.

Description of *eigen-equation.input*:

eigen-equation.input contains input parameters used by **eigne-equation.f**.

Line 1: Total angular momentum L .

Line 2: Total spin.

Line 3: Max angular momentum for each electron l_{\max} .

Line 4: Order of the B-Spline function k .

Line 5: Number of B-SPLINE function knot-points.

Line 6: Total number of the basis sets for the He wavefunction.

Line 7: i_0 in Eq. (31).

Line 8: The simulation box size in radial direction, R_{max} .

Output files of eigen-equation.f: There are two output files after running **eigen-equation.f**: the coefficient c_i of the wavefunction and the eigenvalue E_i .

1. *S.dat* : This file stores the coefficient c_i in Eq.(6). If the input $L = 0$, then the output file is *S.dat*, if $L = 1, 2, 3, 4$, then the output file changes to *P.dat*, *D.dat*, *F.dat*, *G.dat*, respectively.

2. *OMEGA-S.dat*: This file stores the eigenvalue E_i . If the input $L = 0$, then the output file is *OMEGA-S.dat*, if $L = 1, 2, 3, 4$, then the output file changes to *OMEGA-P.dat*, *OMEGA-D.dat*, *OMEGA-F.dat*, *OMEGA-G.dat*, respectively.

B. *dipole.f90*

This program is used to get the dipole matrix element $\sum_{i,j} c_i c_j \langle \varphi_n | (r_1 Y_{10}(\hat{r}_1) + r_2 Y_{10}(\hat{r}_2)) | \varphi_m \rangle$. The subroutines *PREQUAN*, *QUAN2012*, *gauleg*, *RKTSQ*, *Bspline2006* in *dipole.f90* are the same as that in *eigen-equation.f*. The other subroutines in this program are:

ANG: Calculate the angle part of the dipole, G_{ij} .

FE: Calculate $\sqrt{\frac{(1,a,b,c,d)}{4\pi}}$.

Input files of dipole.f90:

1. *dipole.input*

2. the output files *S(P,D,F,...).dat*, *OMEGA-S(P,D,F,...).dat* from **eigen-equation.f** calculations.

Description of *dipole.input*: *dipole.input* contains input parameters used by **dipole.f90**.

Line 1: Total angular momentum of bra $\langle \Psi_{L_{left}} |$ and ket $| \Psi_{L_{right}} \rangle$, respectively.

Line 2: Total spin of bra and ket, respectively.

Line 3: Max angular momentum for each electron l_{max} . This value must be the same as that in Line3 in *eigen-equation.input*.

Line 4: Order of the B-Spline function. This value must be the same as that in Line3 in *eigen-equation.input*.

Line 5: Number of B-SPLINE function knot-points. This value must be the same as that in Line3 in *eigen-equation.input*.

Line 6: Total numbers of the basis sets for bra and ket in the **eigne-equation.f** calculations, respectively. For example, if one uses 240 $L = 0$ basis functions and 425 $L = 1$ basis functions in **eigne-equation.f** calculations, then this line should be 240 425.

Line 7: i_0 in Eq. (31). This value must be the same as that in Line3 in *eigen-equation.input*.

Line 8: The simulation box size in radial direction, R_{max} . This value must be the same as that in Line 3 in *eigen-equation.input*.

Output files of dipole.f90: There is one output file after running **dipole.f90**:

dipole-S-P.dat: This file stores the dipole $\sum_{i,j} c_i c_j \langle \varphi_n | (r_1 Y_{10}(\hat{r}_1) + r_2 Y_{10}(\hat{r}_2)) | \varphi_m \rangle$. If the input variables in the first line of *dipole.input* are 0 1, 1 2, 2 3, 3 4, then the output file should be *dipole-S-P.dat*, *dipole-P-D.dat*, *dipole-D-F.dat* and *dipole-F-G.dat*, respectively.

C. *matrix.f90*

This program is used to put all the dipole matrix elements in matrix H_{nm}^I and energy difference $E_{mn} = E_m - E_n$ in matrix $OMEGA_{nm}$. Table I shows that how we put the matrix elements in H_{nm}^I and $OMEGA_{nm}$.

Input files of matrix.f90:

1. *matrix.input*.
2. the output file of *dipole.f90*: *dipole-S-P*, *dipole-P-D.dat*, *dipole-D-F.dat* and *dipole-F-G.dat*.
3. the output file of *eigen-equation.f*: *OMEGA-S.dat*, *OMEGA-P.dat*, *OMEGA-D.dat*, *OMEGA-F.dat* and *OMEGA-G.dat*.

Description of *matrix.input*: *matrix.input* contains input parameters used by **matrix.f90**.

Line 1: The number of the basis sets of $L = 0$ you want to use in TDSE and the total number of the basis sets of $L = 0$ you got in **eigne-equation.f** calculation, respectively. For example, if you get 240 $L = 0$ basis sets in **eigne-equation.f** calculation, and you only want to use 100 basis sets, you should write down 100 240 in this line.

Line 2: The number of the basis sets of $L = 1$ you want to use in TDSE and the total number of the basis sets of $L = 1$, respectively.

Line 3: The number of the basis sets of $L = 2$ you want to use in TDSE and the total number of the basis sets of $L = 2$, respectively.

Line 4: The number of the basis sets of $L = 3$ you want to use in TDSE and the total number of the basis sets of $L = 3$, respectively.

Line 5: The number of the basis sets of $L = 4$ you want to use in TDSE and the total number of the basis sets of $L = 4$, respectively.

The default max total angular momentum is $L = 4$, user can add larger total angular momentum in this program.

Output files of matrix.f90:

There are three output files after running *matrix.f90*:

1. *eigenval.out*: This file stores all the eigen values of $L = 0, 1, 2, 3, 4$ states.
2. *HI.dat*: This files stores all the dipole matrix elements.
3. *OMEGA.dat*: This files stores all the energy differences.

D. *tdse.f90*

This program is used to calculate the coupled partial differential equations Eq. (9). The subroutines in this program are:

ode: Solve the partial differential equations by Adams algorithm.

f: Describe the laser filed and the partial differential equations.

Input files of tdse.f90:

1. *tdse.input*.
2. *eigenval.out*.
3. *HI.dat*.
4. *OMEGA.dat*

Description of *tdse.input*: *tdse.input* contains input parameters used by **tdse.f90**

Line 1: *HI.dat*, this is the name of the dipole matrix elements file that should be read. Users do not need to modulate it.

Line 2: *OMEGA.dat*, this is the name of the input energy difference file that should be read. Users do not need to modulate it.

Line 3: The maximum number of time steps allowed. Default is 600 000. Usually, users do not need to modulate this value.

Line 4: Frequency of the electric field in atomic unit.

Line 5: Number of the laser cycles.

Line 6: Intensity of the electronic laser field in atomic unit.

Line 7: Relative and absolute errors. Default values are 10^{-7} and 10^{-7} , respectively.

Line 8: No need to change. Besides, users should module the parameter "*NHI*" in **tdse.f90** Line 9 and Line 215. The value of *NHI* should be the total number of the basis functions that you want to use. For example, if you want to use 100 $L = 0$ basis functions, 150 $L = 1$ basis functions, 160 $L = 2$ basis functions, $NHI = 100 + 150 + 160 = 410$.

Output files of **tdse.f90**:

There are four output files after running **tdse.f90**:

1. *laser.dat*: This file stores the laser field $E(t)$.
2. *single-ion.dat*: This file stores the single ionization yield $I_s(t)$.
3. *double-ion.dat*: This file stores the double ionization yield $I_d(t)$.
4. *c.dat*: This file stores the solution $a_n(t)$ of the coupled partial differential equations Eq.(9). Default is outputting all $a_n(t)$. In principle, if we get $a_n(t)$, all the physical information can be retrieved.

E. Other files

There are other five programs **order.f**, **rsg.f**, **wig.f**, **angl16.f90** and **SUBROUTINE.f90** in HeTDSE. These five programs are the "support codes", we **DO NOT** suggest the users to modulate these codes.

IV. SAMPLE RESULTS

In order to check the accuracy of our program, we compare our results with previous literatures. In the calculations, the radius of the cavity is $R_{1max} = R_{2max} = 70$ and it is described by 30 B-Spline functions of order 7. We use $l_{i=1,2} = 0 - 4$ and $L = 0 - 4$. Linear-parabolic knot sequence is chosen because it can balance the accuracy and calculation quantity. 11100 total basis sets are used during the time dependent simulations.

A. *ground and bound states calculation of Helium*

In table 1, we show the eigenvalues of the low bound states for different total angular momenta. Table 1 shows that, for all the calculated levels, at least the accuracy up to two digits after the decimal point has been obtained. The density distributions of different atomic levels in coordinate space are shown in Fig. 3, where the results agree well with that in [19, 37, 38].

B. *excited states dynamics*

Now we turn to the second example: excited states dynamics. Here we focus on the carrier-envelope phase (CEP) effect on band-band state transition induced by a laser pulse. The CEP is a crucial parameter in describing the characteristics of a laser pulse, because we can control the dynamic process of matter-laser interaction by measuring or adjusting the CEP [39–42]. Especially, the CEP effect on the bound-bound transition of an atom has been investigated both in theoretically and experimentally [39–42]. Here we try to reproduce the result from [41]. In [41], the authors used Hylleraas coordinates to reconstruct the wavefunction of Helium, and they introduced a parameter M to quantify the CEP effect:

$$M = \frac{P(\phi_{\max}) - P(\phi_{\min})}{[P(\phi_{\max}) + P(\phi_{\min})]^2}, \quad (32)$$

where $P(\phi_{\max})$ and $P(\phi_{\min})$ are, respectively, the maximum and minimum populations for a given excited state. A large value of M means a strong CEP effect. In this simulation, the laser parameters are the same as [41]. We use HeTDSE get M for 1D after the laser ends, which is shown in Fig 4. Our result matches well with that in Fig.1(b) from [41].

C. *excitation and ionization yields*

Next, we calculate the excitation and ionization yields of helium in a strong laser pulse. Our basis sets covers the energy range located beyond the double-ionization threshold. The initial state is the ground state of Helium $|1S^2\rangle$. The laser pulse has a duration of 3.8 fs and the peak intensity of $2.97 \times 10^{14} \text{W/cm}^2$, which is the same as those in [38, 43]. The present results in Fig. 5 are accordant with the data from Hasbani [43] and Scrinzi [38].

D. *electrons wavepacket dynamics*

We then calculate the electrons wavepacket dynamics both in coordinate and momentum space with different time delay after the laser pulse. The frequency and FWHM of the laser pulse are $\omega = 1.0$ and 2 optical cycles, respectively, with the intensity of $1.0 \times 10^{13} \text{W/cm}^2$. The continue state is collected as $\psi_{ion} = \sum_i c_i \varphi_i$, with $E_i > -2.0 \text{ a.u.}$.

we get the wave function of helium at the end of the laser pulse. Using this wave function, the density distribution of the electrons in coordinate space can be obtained by

$$\rho(r_1, r_2, t) = \int \Psi(r_1, r_2, t) \Psi^*(r_1, r_2, t) r_1^2 r_2^2 d\Omega_1 d\Omega_2. \quad (33)$$

To obtain the wave function in momentum space, we transform the wave function into the momentum space by Fourier transform

$$\Psi(k_1, k_2, t) = \int dr_1^3 dr_2^3 e^{-ik_1 r_1} e^{-ik_2 r_2} \Psi(r_1, r_2, t). \quad (34)$$

By expanding the plane wave $e^{-ik \cdot r}$ as

$$e^{-ik \cdot r} = 4\pi \sum_{lm} (-i)^l j_l(kr) Y_{lm}(k) Y_{lm}^*(r), \quad (35)$$

where $j_l(x)$ is sphere Bessel function,

$$j_l(x) = \sqrt{\frac{\pi}{2x}} J_{l+\frac{1}{2}}(x), \quad (36)$$

the density distribution in momentum space can be obtained by

$$P(k_1, k_2, t) = \int \Psi(k_1, k_2, t) \Psi^*(k_1, k_2, t) k_1^2 k_2^2 d\Omega_1 d\Omega_2. \quad (37)$$

The density distribution of continuous states in coordinate space is shown in Fig. 6 for delay time after the laser ending 0 (a1), 2 (a2), 4 (a3) and 6 (a4) optical cycles. There is an evident single ionization characteristics in the figures, where the wave packet moves outside along the coordinate axis with time. Fig. 7(b1)-(b4) are the corresponding density distributions in momenta space. A red spot in the diagonal direction, with two green branches in the axis direction is found. The red spot implies that the two electrons have an indistinguishability with a same energy. The green branches indicate that electron 1(2) moves with a large(small) velocity. The difference of the red spot in Fig. 7(b1)-(b4) can be attributed to the diffusion of the ionized wave packet in quantum mechanics.

V. PARALLEL SCALING

To test the parallel efficiency of HeTDSE, we compare the serial CPU program (runs at Intel xeon E5-2640 CPU with 2.5GHz clock speed and 15MB L3 cache) and parallel GPU implementations (runs at NVIDIA K20 GPU with 2493 cores). The speedup factor for four simulation cases shown in Table III. The larger the basis number, the larger computation cost needs. All the simulations are done with PGI fortran compiler, the laser is 3.8 fs (which contains about 4000 time steps) and the simulation box is $R_{\max} = 70$. A speed up of 147 is achieved if 4300 basis sets are used. It indicates that as the simulation system size increases, this improvement becomes more and more pronounced.

VI. CONCLUSION

In this work, we present a program which solves the full-dimension-TDSE of helium using OpenACC+GPU simulation acceleration environment. We introduce how to convert the full-dimension-TDSE into coupled partial differential equations. These partial differential equations are solved by Adams method. Our program has two advantages: first, the codes are easily paralleled by adding few detectives and have a speed up of 147 on GPU, HeTDSE dose not have to use a super computer or a computer cluster, even a desktop computer with an openACC-enable GPU can run HeTDSE efficiently; second, we can transplant our program to other accelerators without rewriting the codes. By comparing with the literatures of the excited state dynamics and ionization yield of helium, the accuracy of our program has been verified. Our codes can be used to investigate the non-perturbative electronic dynamics of helium subjected to a strong laser pulse. Besides, for the programming for accelerators such as CUDA is difficult, we hope that HeTDSE to be an example to help more researchers to handle the GPU calculation more easily by using OpenACC.

VII. ACKNOWLEDGEMENTS

CL Wei was supported by the Talent Introduction Foundation of Qiannan Normal University of Nationalities under Grant No. qnsyrc201619 and Natural Science Foundation of Guizhou Provincial Education Department for Young Talents under Grant No. Qian Education Contract KY[2017]339 . Xi Zhao was supported by Chemical Sciences, Geosciences and

Biosciences Division, Office of Basic Energy Sciences, Office of Science, U.S. Department of Energy, under Grant No. DE-FG02-86ER13491.

- [1] T. Shintake *et al*, A compact free-electron laser for generating coherent radiation in the extreme ultraviolet region, *Nat. Photon.* **2** 555(2008).
- [2] W. Ackermann *et al*, Operation of a free-electron laser from the extreme ultraviolet to the water window, *Nat. Photon.* **1** 336(2007).
- [3] M. Hentschel, R. Kienberger, C. Spielmann, G. A. Reider, N. Milosevic, T. Brabec, P. Corkum, U. Heinzmann, M. Drescher, and F. Krausz, Attosecond metrology, *Nature* **414** 509(2001).
- [4] P.M. Paul, E. S. Toma, P. Breger, G. Mullot, F. Augé, P. Balcou, H. G. Muller, and P. Agostini, Observation of a Train of Attosecond Pulses from High Harmonic Generation, *Science* **292** 1689 (2001).
- [5] J. Colgan and M. S. Pindzola, Core-Excited Resonance Enhancement in the Two-Photon Complete Fragmentation of Helium, *Phys. Rev. Lett.* **88** 173002 (2002).
- [6] L. Feng and H. W. van der Hart, Two-photon double ionization of He, *J. Phys. B* **36** L1 (2003).
- [7] S. Laulan and H. Bachau, Correlation effects in two-photon single and double ionization of helium, *Phys. Rev. A* **68** 013409 (2003).
- [8] B. Piraux, J. Bauer, S. Laulan, and H. Bachau, Probing electron-electron correlation with attosecond pulses, *Eur.Phys.J.D* **26** 7 (2003).
- [9] S. X. Hu, J. Colgan, and L. A. Collins, Triple-differential cross-sections for two-photon double ionization of He near threshold, *J. Phys. B* **38** L35 (2005).
- [10] E. Fomouuo, G. L. Kamta, G. Edah, and B. Piraux, Theory of multiphoton single and double ionization of two-electron atomic systems driven by short-wavelength electric fields: An ab initio treatment, *Phys. Rev. A* **74** 063409 (2006).
- [11] X. Guan, K. Bartschat, and B. I. Schneider, Dynamics of two-photon double ionization of helium in short intense xuv laser pulses, *Phys.Rev. A* **77** 043421(2008).
- [12] T.Y. Shi and C. D. Lin, Double Photoionization and Transfer Ionization of He: Shakeoff Theory Revisited, *Phys. Rev. Lett.* **89** 163202(2002).
- [13] H. Hasegawa, E. J. Takahashi, Y. Nabekawa, K. L. Ishikawa, and K. Midorikawa, Multiphoton

- ionization of He by using intense high-order harmonics in the soft-x-ray region, *Phys. Rev. A* **71** 023407 (2005).
- [14] Y. Nabekawa, H. Hasegawa, E. J. Takahashi, and K. Midorikawa, Production of Doubly Charged Helium Ions by Two-Photon Absorption of an Intense Sub-10-fs Soft X-Ray Pulse at 42 eV Photon Energy, *Phys. Rev. Lett.* **94** 043001 (2005).
 - [15] P. Antoine, E. Fomouuo, B. Piraux, T. Shimizu, H. Hasegawa, Y. Nabekawa, and K. Midorikawa, Two-photon double ionization of helium: An experimental lower bound of the total cross section, *Phys. Rev. A* **78** 023415 (2008).
 - [16] A. A. Sorokin, M. Wellhöfer, S. V. Bobashev, K. Tiedtke, and M. Richter, X-ray-laser interaction with matter and the role of multiphoton ionization: Free-electron-laser studies on neon and helium, *Phys. Rev. A* **75** 051402(R) (2007).
 - [17] A. Rudenko, L. Foucar, M. Kurka, Th. Ergler, K. U. Kühnel, Y. H. Jiang, A. Voikov, B. Najjari, A. Kheifets, S. Lüdemann, T. Havermeier, M. Smolarski, S. Schüssler, K. Cole, M. Schöffler, R. Dörner, S. Düsterer, W. Li, B. Keitel, R. Treusch, M. Gensch, C. D. Schröter, R. Moshhammer, and J. Ullrich, Recoil-Ion Momentum Distributions for Two-Photon Double Ionization of He and Ne by 44 eV Free-Electron Laser Radiation, *Phys. Rev. Lett.* **101** 073003 (2008).
 - [18] M. Kurka *et al*, Differential cross sections for non-sequential double ionization of He by 52 eV photons from the Free Electron Laser in Hamburg, FLASH, *New J. Phys.* **12** 073035 (2010).
 - [19] Z. Zhang, L. Y. Peng, M. H. Xu, A. F. Starace, T. Morishita and Q. H. Gong, Two-photon double ionization of helium: Evolution of the joint angular distribution with photon energy and two-electron energy sharing, *Phys. Rev. A* **84** 043409 (2011).
 - [20] Z. Zhang, L. Y. Peng, Q. H. Gong and T. Morishita, Momentum space analysis of multiphoton double ionization of helium by intense attosecond xuv pulses, *Optics Express* **18** 8976 (2010).
 - [21] J. S. Parker, L. R. Moore, K. J. Meharg, D. Dundas and K. T. Taylor, Double-electron above threshold ionization of helium, *J. Phys. B* **34** L69 (2001).
 - [22] J.C. Thibault and I. Senocak, CUDA implementation of a Navier-Stokes solver on multi-GPU desktop platforms for incompressible flows, in: Proceedings of the 47th AIAA Aerospace Sciences Meeting, Orlando, Florida, USA, 2009.
 - [23] NVIDIA CUDA ZONE. <https://developer.nvidia.com/cuda-zone>. version 4.0, 2011.
 - [24] Y. Komura, OpenACC programs of the Swendsen-Wang multi-cluster spin flip algorithm,

- Comput. Phys. Commun.* **197** 298 (2015).
- [25] J.E. Stone, J.C. Phillips, P.L. Freddolino, D.J. Hardy, L.G. Trabuco, K. Schulten, Accelerating molecular modeling applications with graphics processors, *J. Comput. Chem.* **28** (2007) 2618.
 - [26] W. L. Cheng, A. Sheharyar, R. Sadr and O. Bouhali, Application of GPU processing for Brownian particle simulation, *Comput. Phys. Commun.* **182** 39 (2015).
 - [27] C. Broin and L.A.A. Nikolopoulos, A GPGPU based program to solve the TDSE in intense laser fields through the finite difference approach, *Comput. Phys. Commun.* **184** (2014) 1791.
 - [28] T. D. Nguyen, GPU-accelerated Tersoff potentials for massively parallel Molecular Dynamics simulations, *Comput. Phys. Commun.* **212** 113 (2017).
 - [29] L. Exl, A GPU accelerated and error-controlled solver for the unbounded Poisson equation in three dimensions, *Comput. Phys. Commun.* **221** 352 (2017).
 - [30] OpenACC. <http://www.openacc-standard.org/>.
 - [31] M. Venuti and P. Decleva, Convergent multichannel continuum states by a general configuration interaction expansion in a B-spline basis: application to H- photodetachment, *J. Phys. B* **30** 4839 (1997).
 - [32] H. Bachau, E. Cormier, P. Decleva, J. E. Hansen and F. Martín, Applications of B-splines in atomic and molecular physics, *Rep. Prog. Phys.* **64** 1815 (2001).
 - [33] Xi Zhao, Hui Wei, Yan Wu and C. D. Lin, Phase-retrieval algorithm for the characterization of broadband single attosecond pulses, *Phys.Rev. A* **95** 043407 (2016).
 - [34] Xi Zhao, Hui Wei, Changli Wei and C D Lin, A new method for accurate retrieval of atomic dipole phase or photoionization group delay in attosecond photoelectron streaking experiments, *J. Opt.* **19** 114009 (2017).
 - [35] T. Y. Shi, C. G. Bao and B.W. Li, Energy Spectra of the Confined Atoms Obtained by Using B-Splines, *Commun. Theor. Phys.* **35** 195(2001).
 - [36] J. N. Massot, E. Elbaz and J. Lafoucriere, A General Graphical Method for Angular Momentum, *Rev. Mod. Phys.* **39** 288 (1967).
 - [37] Z. Zhang 2012, Two-photon double ionization of helium by solving full-dimentional TDSE Ph. D. Dissertation (Beijing: Peking University).
 - [38] A. Scrinzi and B. Piraux, Two-electron atoms in short intense laser pulses, *Phys.Rev. A* **58** 1310 (1998).
 - [39] H. Li, V. A. Sautenkov, Y. V. Rostovtsev, M. M. Kash, P. M. Anisimov, G. R. Welch, and M.

- O. Scully, Carrier-Envelope Phase Effect on Atomic Excitation by Few-Cycle rf Pulses, *Phys. Rev. Lett.* **104** 103001 (2010).
- [40] Xi Zhao, Jing Chen, Panming Fu, Xueshen Liu, Zong-Chao Yan, and Bingbing Wang, Carrier-envelope-phase effect in a long laser pulse with tens of optical cycles, *Phys.Rev. A* **87** 043411 (2013).
- [41] Dian Peng, Biao Wu, Panming Fu, Bingbing Wang, Jiangbin Gong and Zong-Chao Yan, Sensitive frequency dependence of the carrier-envelope phase effect on bound-bound transitions: An interference perspective, *Phys.Rev. A* **82** 053407 (2010).
- [42] T. Nakajima and S. Watanabe, Effects of the Carrier-Envelope Phase in the Multiphoton Ionization Regime, *Phys. Rev. Lett.* **96** 213001 (2006).
- [43] R. Hasbani, E. Cormier and H. Bachau, Resonant and non-resonant ionization of helium by XUV ultrashort and intense laser pulses, *J. Phys. B* **33** 2101 (2000).

```
!$acc parallel loop
do i = 1, n
  b(i) = a(i)+b(i)
enddo
```

FIG. 1: (Color online) A typical fortran openACC program

TABLE I: Order of the dipole matrix element and energy difference. The number of the basis function for $L = 0$, $L = 1$ and $L = 2$ is N_0 , N_1 and N_2 respectively.

$H_{nm}^I(n, m)$	L=0	L=1	L=2	...
L=0	0	$H_{nm}^I \left(\begin{matrix} n = N_0 + 1, N_0 + N_1 \\ m = 1, N_0 \end{matrix} \right)$ $OMEGA \left(\begin{matrix} n = N_0 + 1, N_0 + N_1 \\ m = 1, N_0 \end{matrix} \right)$	0	
L=1	$H_{nm}^I \left(\begin{matrix} n = 1, N_0 \\ m = N_0 + 1, N_0 + N_1 \end{matrix} \right)$ $OMEGA \left(\begin{matrix} n = 1, N_0 \\ m = N_0 + 1, N_0 + N_1 \end{matrix} \right)$	0	$H_{nm}^I \left(\begin{matrix} n = N_0 + N_1 + 1, N_0 + N_1 + N_2 \\ m = N_0 + 1, N_0 + N_1 \end{matrix} \right)$ $OMEGA \left(\begin{matrix} n = N_0 + N_1 + 1, N_0 + N_1 + N_2 \\ m = N_0 + 1, N_0 + N_1 \end{matrix} \right)$	
L=2	0	$H_{nm}^I \left(\begin{matrix} n = N_0 + 1, N_0 + N_1 \\ m = N_0 + N_1 + 1, N_0 + N_1 + N_2 \end{matrix} \right)$ $OMEGA \left(\begin{matrix} n = N_0 + 1, N_0 + N_1 \\ m = N_0 + N_1 + 1, N_0 + N_1 + N_2 \end{matrix} \right)$	0	
...				

TABLE II: The energy level of some bound states.

Helium states	Our results	Ref. [38]	Ref. [19]	Ref. [37]
1 ¹ S	-2.900029	-2.903531	-2.903669	-2.903724
2 ¹ S	-2.145044	-2.145961	-2.145970	-2.145974
3 ¹ S	-2.060512	-2.061268	-2.061271	-2.061272
4 ¹ S	-2.032866	-2.033585	-2.033585	-2.033587
2 ¹ P	-2.123121	-2.123832	-2.123839	-2.123843
3 ¹ P	-2.054443	-2.055143	none	none
3 ¹ D	-2.054927	-2.055621	-2.055555	-2.055620
4 ¹ D	-2.030586	-2.031280	none	none
4 ¹ F	-2.030562	-2.031255	none	none
5 ¹ F	-2.019272	-2.020003	none	none

TABLE III: The efficiency of our GPU program.

Basis number	GPU time	CPU time	Speed-up ratio
3000	41.22	3644.07	88.41
3600	48.61	4963.76	102.11
4200	60.06	7278.36	121.18
4800	86.26	12625.83	146.37

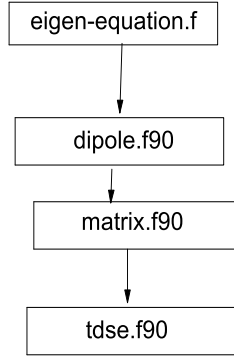


FIG. 2: (Color online) The program construct of HeTDSE. The arrow \rightarrow from program A to program B corresponding that, the output file from A is used as a input file in program B.

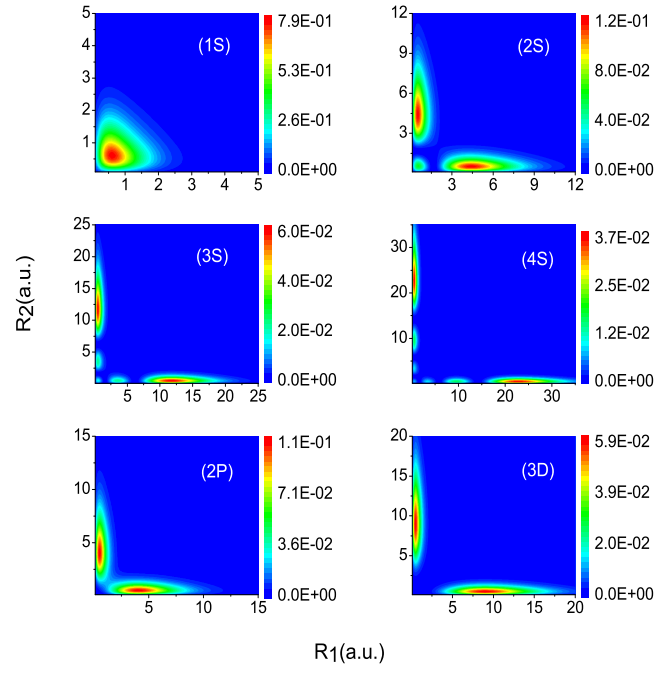


FIG. 3: (Color online) The density distributions of some bound states in coordinate space.

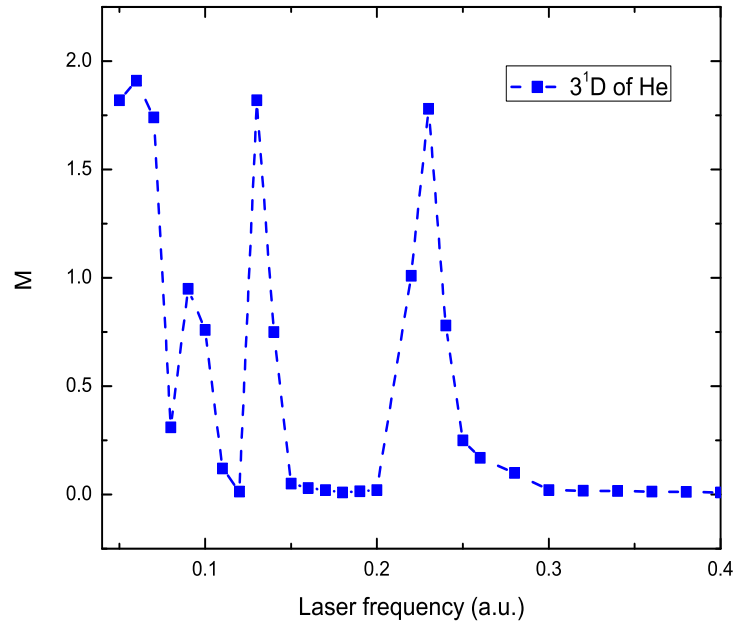


FIG. 4: (Color online) The CEP parameter M vs the laser frequency for 3^1D state of helium.

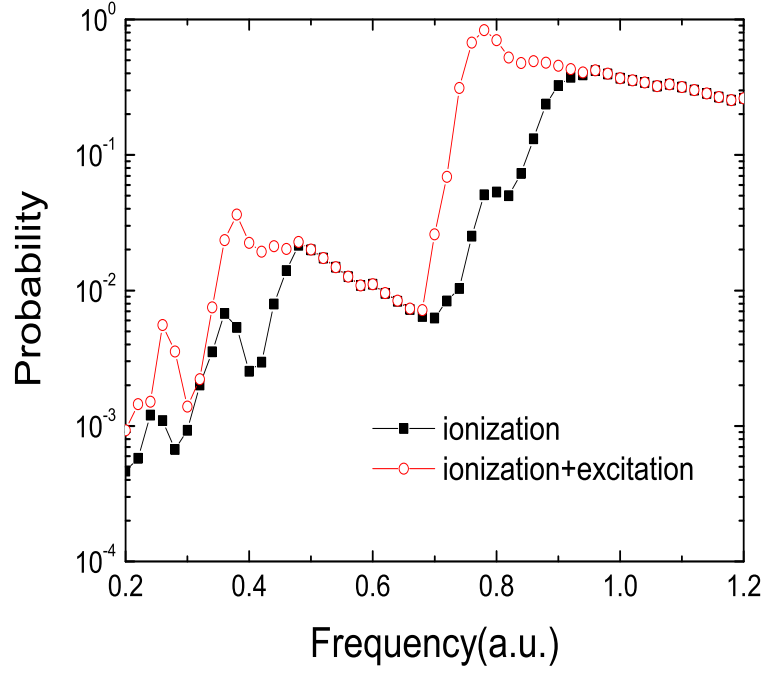


FIG. 5: (Color online) Excitation and ionization probabilities, for the helium atom, with a pulse duration of 3.8 fs (fixed) and a peak intensity of $2.96 \times 10^{14} W/cm^2$.

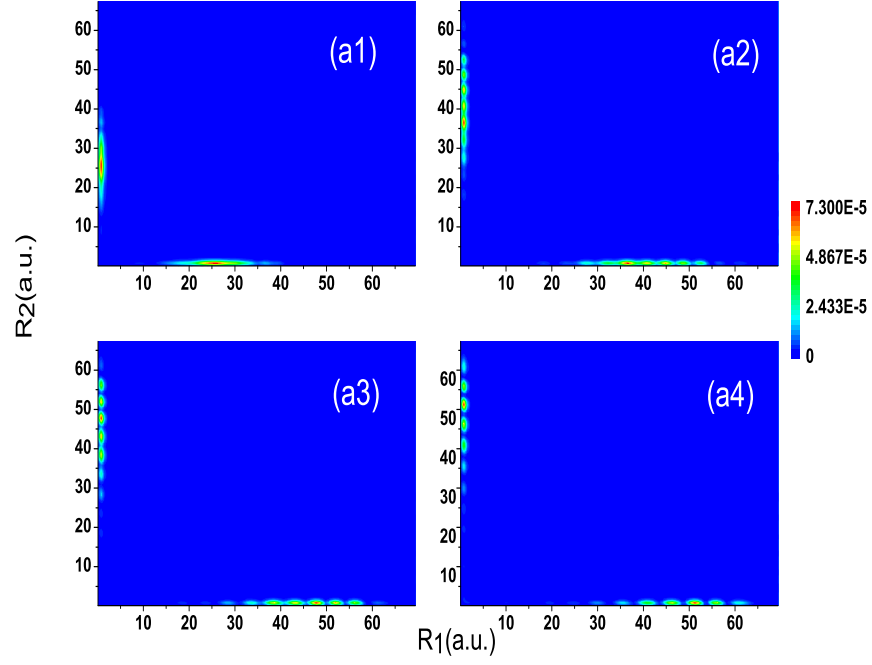


FIG. 6: (Color online) The distributions of the continuum state in the coordinate space $\omega = 1.0$, FWHM=2 OC, intensity $I = 1.0 \times 10^{13} \text{ W/cm}^2$, the time delay after laser ending is 0 OC(a1), 2 OC(a2), 4 OC(a3), 6 OC(a4).

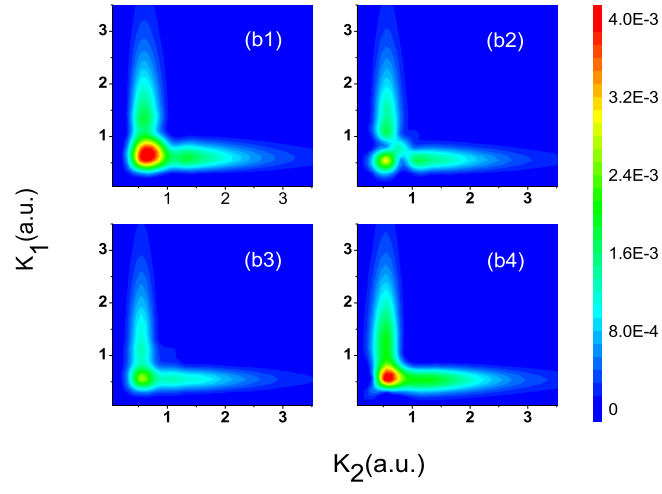


FIG. 7: (Color online) The distributions of the continuum state in the momentum space $\omega = 1.0$, FWHM=2 OC, intensity $I = 1.0 \times 10^{13} W/cm^2$, the time delay after laser ending is 0 OC(b1), 2 OC(b2), 4 OC(b3), 6 OC(b4).